

# Control of Natural Tollmien-Schlichting Waves using Dielectric Barrier Discharge Plasma Actuators

Marios Kotsonis, Ram Krishan Shukla and Stefan Pröbsting  
Delft University of Technology, The Netherlands  
E-mail: m.kotsonis@tudelft.nl

## ABSTRACT

An experimental investigation on active control of naturally occurring Tollmien-Schlichting (TS) instabilities on a NACA 0012 airfoil is presented. A real-time closed-loop control system has been implemented using the filtered-x Least Mean Squares (FXLMS) adaptive algorithm based on Finite Impulse Response (FIR) filters. Two surface mounted microphones provide the unsteady surface pressure measurements, which are used as reference and error signal, respectively. The controller directly drives a Dielectric Barrier Discharge plasma actuator positioned on the suction side of the airfoil. In contrast to the conventionally modulated sinusoidal signal, the actuator is powered using a signal continuously adapted in real time by the controller. In this manner, the inherently unsteady plasma force production is capitalised in order to dampen the incoming wave-train of Tollmien-Schlichting instabilities. Time-resolved two-component Particle Image Velocimetry is used to characterize the flow in the vicinity of the actuator. Several cases are tested using both open- and closed-loop actuation. In the case of open-loop control, the actuator is operated with a non-adapted single-frequency sinusoidal signal. Freestream velocity ranges from 17 to 25 m/s, equivalent to a chord based Reynolds numbers between  $0.2$  to  $0.35 \times 10^6$  respectively. The experimental results indicate a suppression of the discrete component of the unstable TS waves with closed-loop actuation. A maximum amplitude reduction of approximately 50% is achieved at low velocities. In contrast, open-loop control appears to accentuate the growth of discrete instability modes when the frequency of actuation is in the instability region for the given conditions. An additional stretching effect is observed on the TS waves for both open- and closed-loop control as a result of the inherently directional plasma body force.

**Key Words:** natural TS waves; active control; DBD plasma; FXLMS algorithm; direct frequency mode

## 1. INTRODUCTION

Active cancellation of laminar boundary layer instability waves has been a topic of interest in recent years. The growth of boundary layer instability waves eventually leads to laminar-turbulent transition, with an associated increase in skin friction drag. Direct control of the latter can provide an efficient mechanism towards transition delay and drag reduction in 2D flows typically encountered over airfoils.

A number of researchers have attempted the direct cancellation of laminar boundary layer instability waves experimentally: Milling, (1981) and Liepmann and Nosenchuck (1982) demonstrated successful attenuation of Tollmien-Schlichting (TS) instabilities in an early linear stage by superposition with anti-phase waves. These experiments were conducted using artificial single-frequency disturbances produced by periodic heating of flush-mounted heating elements. Thomas (1983) studied the cancellation of travelling waves in a boundary layer on a zero pressure gradient flat plate model using electromagnetic generators. He demonstrated damping of the two-dimensional (2D) disturbance, reducing their amplitude to 20%. Ladd and Hendricks (1988) conducted an experimental study of adaptive heating on 2D instabilities in a laminar boundary layer on an axisymmetric body (ellipsoid) in a water tunnel. However, Ladd and Hendricks (1988) noted that the naturally occurring waves on an ellipsoid are highly

three-dimensional (3D), thus complicating cancellation. Pupator and Saric (1989) and Ladd (1990) investigated the development and cancellation of random disturbances over a flat plate and axisymmetric body in a wind and water tunnel. They applied an active feedback control loop for the cancellation of broadband disturbances by generating counter disturbances based on appropriate transfer functions. Sturzebecher and Nitsche (2003) measured the evolution and spatial amplification of TS waves. They reported suppression of artificially excited and natural TS waves using “active skin” sensors, actuators and adaptive controllers using the FXLMS algorithm. Grundmann and Tropea (2008) demonstrated the attenuation of artificially introduced TS waves by imparting steady and unsteady forces to the boundary layer with an arrangement of Dielectric Barrier Discharge (DBD) plasma actuators.

DBD actuators offer a promising actuation concept for the control of unsteady flow instabilities. They consist of two electrodes separated by a dielectric layer. By applying an AC high voltage signal between the two electrodes a locally strong electric field develops, which in turn ionizes the surrounding air in the vicinity of the actuator. Through collisional processes the ionized gas (plasma) transfers momentum to the flow, which can be used for control (Moreau, 2007). In addition to mechanical simplicity and robustness, low power consumption and cost efficiency, a major advantage is their extremely fast response time. Typical response times of these actuators can reach up to several milliseconds due to the lack of mechanical parts.

The high voltage used to power these actuators is typically driven at a *carrier frequency* on the order of 1–10 kHz. Several methods have been developed to drive this voltage. Most commonly, the carrier frequency is modulated with a lower frequency (10–100 Hz) square or sine wave. This signal causes the actuator to switch on and off at a given *modulation frequency*, matching that of the unsteady hydrodynamic mechanism subject to control. A typical application example is the control of TS waves (Grundmann and Tropea, 2008). Although this technique has been shown to be effective for certain cases, disadvantages arise when the modulation frequency and the carrier frequency attain similar values. This effectively means that an upper bound exists on the frequency regimes the modulation method can reach.

More recently, Kotsonis and Ghaemi (2011) demonstrated the ability of the actuator to produce an unsteady forcing effect directly related to the carrier frequency and showed the frequency of the unsteady forcing to match the carrier frequency. Moreover, the actual shape of the waveform of the applied voltage was shown to affect the forcing. Using the carrier signal to directly control flow instabilities has some advantages over the conventional modulation technique: firstly, the upper bound for the actuation frequency is considerably higher than for the modulation method. Secondly, the actuation can be tailored using advanced control algorithms, which adapt not only the frequency and phase of actuation but also the shape of the applied waveform. The main disadvantage of directly using the carrier frequency is the non-linear relationship between applied voltage and force magnitude (Moreau, 2007). As such, amplitude control requires complex control algorithms compared to the frequency modulation technique. Kurtz et al. (2012) have demonstrated the working principle of direct control for the simple case of single-frequency artificially introduced TS waves. To date, the use of this technique in a truly closed loop control scheme has not been reported.

Concurrently to the experimental approaches, numerical research has led to the advancement of control algorithms. Joslin et al. (1995) performed Direct Numerical Simulations (DNS) based on a spectral control approach and demonstrated the attenuation of TS waves with a sensor-actuator arrangement on a flat plate. Herbert et al. (1996) attempted the attenuation of TS disturbances, using a neural network. Baumann et al. (1996, 1997, 2000) utilized an adaptive linear control algorithm based on a fast signal processor and applied this for effective dampening of natural TS instabilities on an airfoil. Gmelin et al. (2000) presented dampening of linear instabilities by means of actuation in combination with Finite Impulse Response (FIR filters) and described the concepts of the nonlinear methods for reducing the resonant behavior of 2-D and 3-D instability modes. Albrecht et al. (2007) performed numerical simulations where they demonstrated the phase opposition control of TS waves by Lorentz forces. Kotsonis et al. (2013) reported a numerical investigation on the dampening of single- and multi-frequency TS waves using an adaptive control system based on the filtered-x LMS algorithm (Kuo and Morgan, 1996). The control system employed the unsteady surface pressure signal in order to determine frequency, phase and amplitude of the opposing plasma body force to reduce the amplitude of propagating TS waves. Results showed large reductions in wave amplitude.

It is evident that the state-of-the-art in active cancellation of TS waves consists of a variety of approaches both on the control algorithm level and the actuator level. This study combines DBD plasma actuators with an advanced control algorithm and demonstrates the direct control of naturally

occurring TS waves on an airfoil. Additionally, the inherently unsteady nature of plasma induced forcing is used to directly control the incoming instability waves without the commonly used signal modulation associated with unsteady plasma control. This provides means for the control of unsteady fluctuations at frequencies of several kilohertz.

## 2. EXPERIMENTAL SETUP

### 2.1. Airfoil and Wind Tunnel Facility

A NACA 0012 airfoil of chord length 200 mm and span 400 mm was mounted vertically in the low-speed vertical open jet facility (V-tunnel) at Delft University of Technology. The wind tunnel has a circular open jet outlet of diameter 600 mm, maximum velocity of 40 m/s and a high contraction ratio (100:1), which enables free stream turbulence values well below 0.1 %. Polycarbonate side plates of diameter 300 mm were placed on the sides of the airfoil in order to ensure two-dimensionality for the mean flow and allow for optical access. A general schematic of the experimental setup is shown in Fig. 1. The tests were performed at free stream velocities of 17, 20, and 25 m/s (equivalent to  $Re_c = 0.22, 0.27$  and  $0.33 \times 10^6$ ) at geometric angle of attack of  $2^\circ, 1.7^\circ$  and  $-0.6^\circ$ , respectively. These conditions were selected in order to ensure growth of TS waves in the region of actuation. Three-dimensional roughness elements (carborundum, nominal grain size of 0.84 mm) were applied near the trailing edge of the airfoil (suction side) to suppress tonal noise from coherent instability waves scattering at the trailing edge (Plogmann et al., 2013; Pröbsting et al., 2014). The airfoil was manufactured from polycarbonate to prevent electrical arcing from the operation of the plasma actuator. Microphone cabling inside the airfoil was shielded with conductive fabric and Electro-Magnetic Interference (EMI)-suppressing paint in order to minimize electromagnetic interference on the microphones.

Seven electret condenser Sonion 8010-T microphones were located at the mid-span of the airfoil at chordwise positions spanning from  $x/c = 0.1$  to 0.8. The microphones were embedded in a shielded cavity, within the body of the airfoil, and connected to the surface through pinholes of diameter 0.1 mm to measure the unsteady surface pressure. The microphones were simultaneously sampled using a 16-bit A/D compact DAQ system from National Instruments at a frequency of 100 kHz. Additionally, microphones 5 and 6, located at  $x/c = 0.55$  and  $x/c = 0.65$  respectively provided reference and error signals for the adaptive control system (Fig. 2). The output of the different microphone readings was equalised using a loudspeaker.

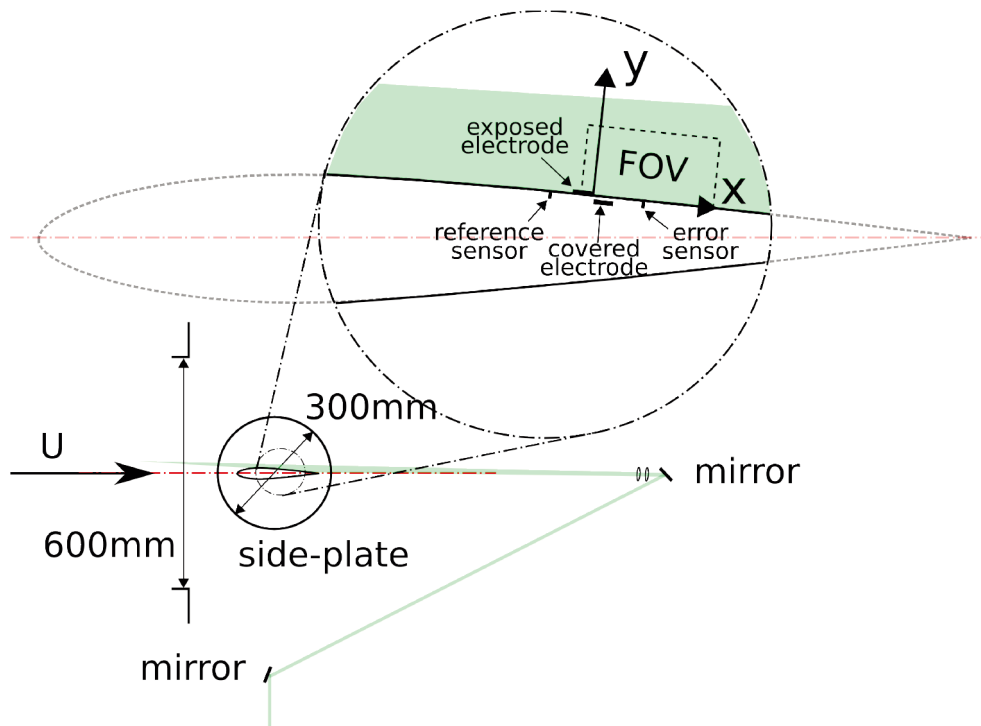


Figure 1. Schematic of the experiment arrangement in V-Tunnel. (not to scale).

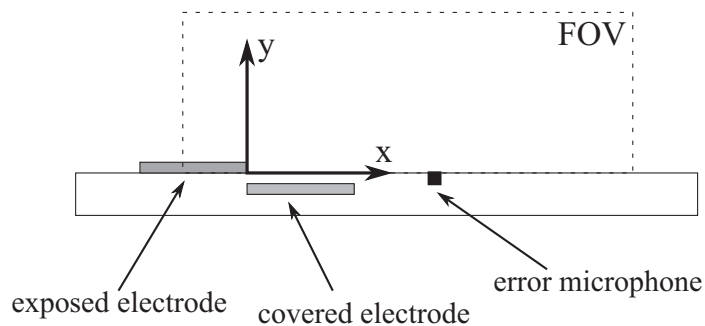


Figure 2. Positioning of the plasma actuator and general coordinate system.

## 2.2. DBD Plasma Actuator

For control of the evolving TS waves, a DBD plasma actuator was positioned on the suction side of the airfoil. (Fig. 2). The actuator consisted of two copper electrodes, separated by polyimide dielectric (Kapton), directly attached on the surface of the airfoil. Thin rectangular copper electrodes were employed consisting of self-adhesive copper tape. The thickness was  $30\ \mu\text{m}$  including adhesives. Two dielectric layers of Kapton tape (thickness  $50.8\ \mu\text{m}$  each) separated the two electrodes, resulting in a total thickness of the actuator below  $130\ \mu\text{m}$ . The protruding step due to the actuator was filled and smoothed using putty and thin tape. Preliminary measurements have shown that the introduced step had no significant effect on the transition process. The streamwise length of both the exposed and covered electrodes was  $5\ \text{mm}$ . The spanwise length (along which plasma is formed) was approximately  $200\ \text{mm}$ . No horizontal gap was formed between the electrodes. The exposed electrode was powered using a TREK 20/20 C high-voltage (HV) amplifier, while the covered electrode was kept at ground potential. The driving HV signal was produced directly by the adaptive controller and by a digital function generator for the closed- and open-loop test cases, respectively. For the open-loop control sinusoidal signals of  $5\ \text{kV}$  amplitude were used at various carrier frequencies. The actuator was positioned between the reference and error microphones such that the interface line of the two electrodes was located at  $x/c = 0.6$ .

## 2.3. PIV Measurements

A Photron Fastcam SA1.1 high-speed CMOS camera ( $5.4\ \text{kHz}$  at  $1\ \text{Mpx}$ ,  $20\ \mu\text{m}$  pixel pitch) was used to capture the field of view (FOV). Image pairs, were recorded at  $5.4\ \text{kHz}$  (closed- and open-loop control case). The camera was equipped with a Nikon Micro-Nikkor  $200\ \text{mm}$  objective. The aperture number ( $\#$ ) was set to 4 and the field of view (FOV) enclosed a window of  $32\ \text{mm} \times 16\ \text{mm}$  at a magnification factor of  $M = 0.64$ . The synchronization between laser and camera was performed using a LaVision High-Speed controller and Davis 8 software package. Seeding particles based on non-toxic water-glycol mixture of approximately  $1\ \mu\text{m}$  diameter were entrained in the flow. The particles in the mid-span plane were illuminated by a light sheet of about  $2\ \text{mm}$  thickness emitted by a Quantronix Darwin- Duo laser (maximum energy of  $30\ \text{mJ}$  per pulse at  $2\ \text{kHz}$ ).

Image sequences were analysed using Davis 8 by multi-grid, multi-pass cross-correlation. A final interrogation window size of  $16 \times 16$  pixels with  $75\%$  overlap resulted in a final vector spacing of  $8$  vectors/mm (window size  $0.5\ \text{mm}$ ). Due to the large radius of curvature of the airfoil and the comparatively small field of view a Cartesian coordinate system approximates the surface attached coordinate with origin at the actuator. The coordinate system is shown in Fig. 2.

## 3. FXLMS ADAPTIVE CONTROL SYSTEM

A control system based on the filtered-x LMS (FXLMS) adaptive algorithm was devised and applied for the control task. The concept is derived from active noise cancellation techniques and involves a feedforward loop for the estimation of the control signal, which drives the actuator (Kuo and Morgan, 1996). A schematic of the working principle is provided in Fig. 3. The system mainly comprises the reference sensor (surface microphone upstream of the actuator), error sensor (surface microphone downstream of the actuator), plasma actuator and adaptive control algorithm. The system uses a primary Finite Impulse Response (FIR I) filter, which accepts the instantaneous reference signal  $x(k)$  as input and produces the instantaneous output signal  $y(k)$  (equation 1), where  $k$  is the index of the last sample of the reference signal and  $L$  is the length of the primary FIR filter defined by  $w^l$ :

<sup>1</sup>The notation of Hansen (2001) is followed. Bold face denotes vector variables.

$$y(k) = \mathbf{w}(k)^T \mathbf{x}(k) = \sum_{i=1}^{L-1} w_i(k) x(k-i) \quad (1)$$

Note that  $\mathbf{w}(k) = [w_1(k) w_2(k) \dots w_{L-1}(k)]^T$  is a finite impulse filter vector and  $\mathbf{x}(k) = [x(k) x(k-1) \dots x(k-L+1)]^T$  is a vector containing the  $L$  chronologically last samples of the reference signal. The output signal is sent to the amplifier and directly drives the actuator. This implies that the controller determines the amplitude, frequency, and phase of the control signal.

The Least Mean Squares (LMS) algorithm provides the optimal weight vector based on the minimization of the mean square  $E[e^2(k)]$  of the error signal  $e(k)$ , which is measured by the error sensor. In the control algorithm,  $f(k)$  is produced by filtering the reference signal with a secondary FIR filter (FIR II) which is a digital representation of the natural cancellation path. This is done in order to have a valid comparison between reference and error signals for the update process by taking into account the changes in phase, frequency and amplitude of the instabilities between reference and error microphone.

The cancellation path copy (FIR II) is obtained using a System Identification (SI) routine based on a modified version of the LMS adaptive algorithm. More specifically, the actuator is driven by a predetermined signal, which in this case is a stored time series of the reference signal  $x(k)$  (effectively applying a large delay on the incoming signal). At the same time  $x(k)$  is passed through the secondary filter. The produced signal is then subtracted from the error signal and used in the LMS routine to update the coefficients of FIR II. By using the difference of the two signals to update FIR II, the final weight coefficients of the secondary filter are such that the instantaneous values of the predicted and actual error signal are the same ( $f(k) = e(k)$ ). This effectively means that FIR II can model the natural cancellation path as it was initially required by the primary control system. As soon as the System Identification (SI) algorithm converges and FIR II is available the control sequence can begin. It must be noted here that several choices can be made regarding the type of predetermined actuator driving signal for SI. More specifically, this signal can be either random noise or a signal with the same spectral content as the incoming disturbances. The second method was chosen in this study and the reference signal itself was used. The advantage of using the reference signal is that no additional noise is introduced into the system and implementation using the real-time controller (see below) is relatively straightforward. The disadvantage is that the control signal becomes highly correlated with the reference signal, which causes errors in the transfer function estimation. In the present study, this is not an issue since the wind tunnel is operating at constant speed and as such the spectral content of the incoming instabilities is not changing. On the other hand, for a more realistic application, such as the wing of an aircraft, SI based on random noise predetermined signals should be preferred due to increased robustness.

Continuous adaptation of the weighting vector (equation 2) results in the desired cancellation effect:

$$\mathbf{w}(k+1) = \mathbf{w}(k) - 2\mu e(k) \mathbf{f}(k) \quad (2)$$

Note that the convergence coefficient  $\mu$  is normalized as shown in equation 3, where convergence factor  $\beta$  is a constant. This normalisation is performed in order to decouple the performance of the controller from the amplitude of the reference signal.

$$\mu = \frac{\beta}{\mathbf{x}(k)^T \mathbf{x}(k)} \quad (3)$$

A further correction is performed considering that due to the fixed-point mathematics used by the real-time controller, error accumulation can be a potential threat to the stability of the adaptation process. A leaky-FXLMS algorithm (also known as tap leakage) is applied to overcome the instability by relaxation in the update of the weighting vector  $\mathbf{w}$ , where  $\alpha$  is a small positive number referred to as leakage coefficient. Under these parameters the update procedure is given by:

$$\mathbf{w}(k+1) = \mathbf{w}(k) [1 - \mu\alpha] - 2\mu e(k) \mathbf{f}(k) \quad (4)$$

A larger convergence coefficient  $\mu$  renders the algorithm unstable, while small  $\mu$  makes the convergence slower but ensures stability. The convergence coefficient is selected by trial and error and depends on the application at hand. A general schematic of the control algorithm is shown in Fig. 3, while a general schematic of the SI process is given in Fig. 4.

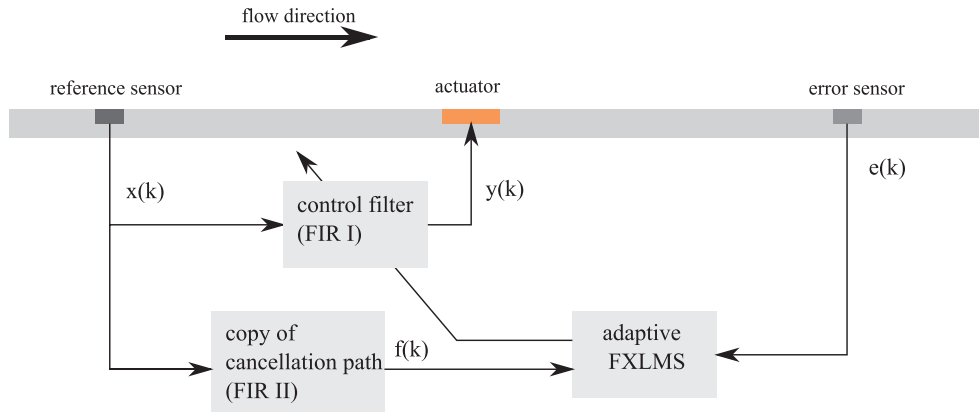


Figure 3. Schematic for the FXLMS control algorithm.

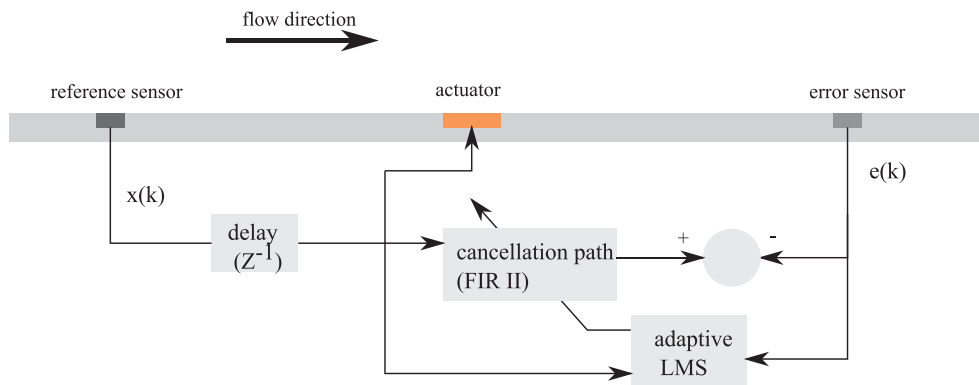


Figure 4. Schematic for the System Identification (SI) algorithm (the saved time series of the reference signal is represented by a delay ( $Z^{-1}$ )).

The control algorithm has been implemented in a real-time Field Programmable Gate Array (FPGA) system (National Instruments compact Reconfigurable Input Output (c-RIO)) cycling at 10 kHz. The sampling of the reference and error microphones takes place at 10 kHz. Simultaneously, the microphones are also sampled at 100 kHz for logging purposes. The update of the FIR filters is performed at 1 kHz in order to allow sufficient time between the moment of actuation and the detection of the resulting effect. The c-RIO is communicating to the reference and error microphones using 16-bit A/D modules while it drives the actuator by sending voltage signal to the HV amplifier via a 16-bit D/A module. After the initiation of the control sequence the system automatically performs system identification and control with no further user input. For the majority of the closed loop control 50 taps (coefficients) were used for FIR I and FIR II with a convergence factor  $\beta = 0.3$ .

## 4. RESULTS AND DISCUSSION

### 4.1. Base Flow

The developed flow has been characterised using time-resolved PIV measurements. Prior to the controlled cases the base flow was identified. Fig. 5 shows the non-actuated flow developed at the suction side of the airfoil for free stream velocities of 17 and 25 m/s. It is evident from the integral boundary layer parameters that the boundary layer at these conditions is laminar. Additionally, the shape factor and the velocity profiles indicate a strong momentum deficit rendering the boundary layer highly inflectional. Nevertheless, careful inspection of the ensemble average reveals no sign of separation.

### 4.1. Open-Loop Control

In the open loop control case, the actuator is operated using a non-adapted sinusoidal signal in order to investigate the development of the unstable TS waves at different carrier frequencies. The amplitude of

this signal is 5 kV at all selected carrier frequencies. Statistics of the velocity field in this section have been obtained by averaging over a measurement period of approximately 1 s.

Instantaneous snapshots with contours of streamwise and wall-normal velocity fluctuation ( $u'$  and  $v'$ ) are depicted in Fig. 6 for the case of no actuation at free-stream velocity  $U_0 = 17$  m/s. A convecting train

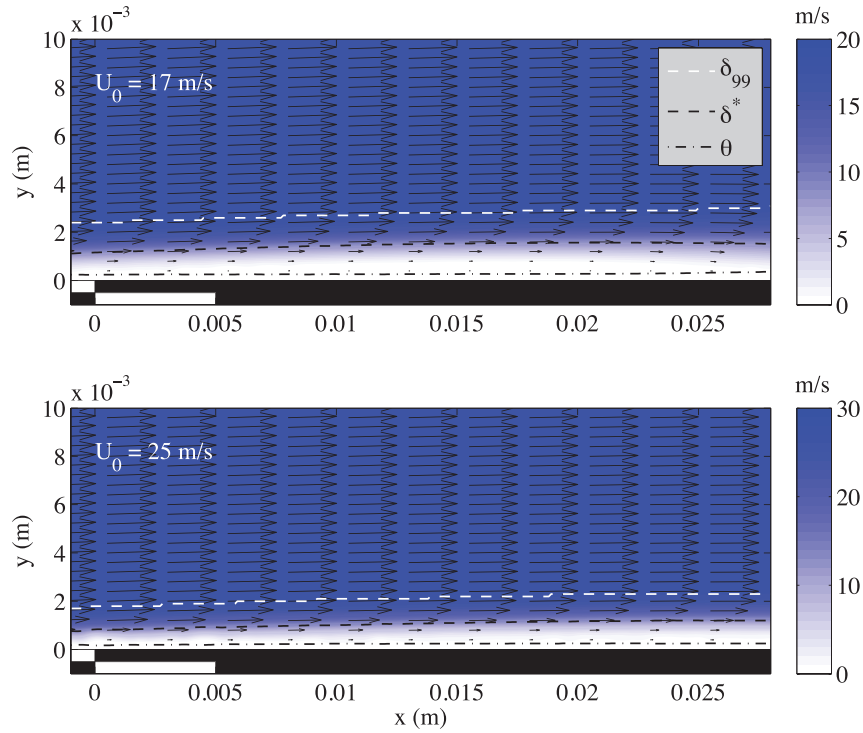


Figure 5. Time averaged velocity fields for  $U_0 = 17$  m/s and  $U_0 = 25$  m/s and boundary layer parameters.

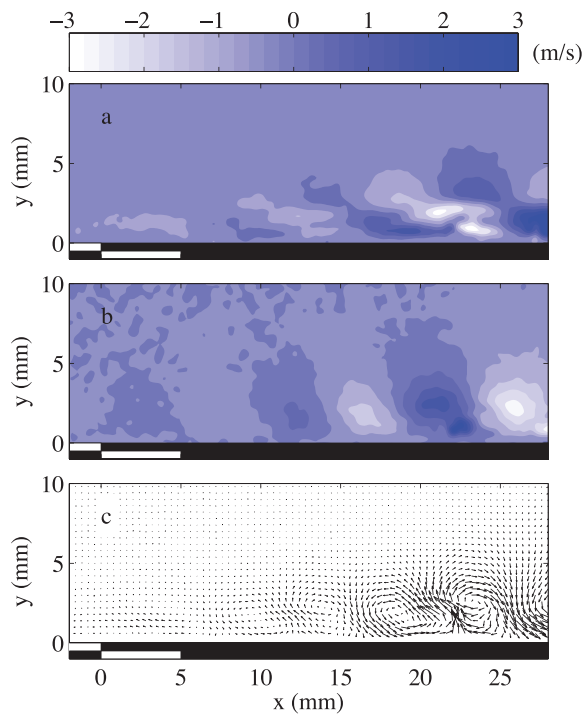


Figure 6. Instantaneous (a) streamwise and (b) wall-normal velocity fluctuations for the case of  $U_0 = 17$  along with (c) corresponding vector field of the instantaneous fluctuating velocity field.

of instability waves is evident, with increasing amplitude in the streamwise direction. The waves are characterised by a double peak motion in the streamwise direction accompanied by a single peak transverse motion in the wall normal direction. The vector field illustrates the motion as counter rotating vortices convecting downstream in the laminar boundary layer. These features identify the observed waves as Tollmien-Schlichting (TS) modes (Pupator and Saric, 1989). The relatively large amplitude ( $>1\%$  rms of the free stream velocity) suggests non-linear interaction for most of the downstream portion of the observation field ( $x > 5$  mm).

Complementing the statistical analysis, the diagonal components of the Reynolds stress tensor are estimated by the Root Mean Square (RMS) of the velocity fluctuations and presented for  $U_0 = 17$  m/s (Fig. 7) and  $U_0 = 25$  m/s (Fig. 8). Fig. 9 shows the development of maximum RMS of velocity fluctuations along the streamwise direction. The profiles of streamwise fluctuations confirm a double peak structure, typical of 2D TS waves.

Open-loop control is applied by operating the actuator at various carrier frequencies. The development of the velocity fluctuations is highly dependent on the frequency of actuation. The profile shows higher fluctuations values at carrier frequency of 850 Hz while significantly reduced values compared to the baseflow are evident at 1500 Hz. Similarly, at  $U_0 = 25$  m/s an actuation frequency of 1500 Hz enhances the fluctuation intensity while 3000 Hz suppress it compared to no actuation. The high amplitude of fluctuations at the downstream positions of the FOV should be noted here. Typical RMS values at  $x = 28$  mm are in the order of 10 % of the freestream velocity. Although this large amplification results in waves of sufficiently large amplitude to be observed with the present PIV set-up, it also indicates non-linear interaction. On the other hand, instability waves passing over the actuator (at  $x = 0$  mm) are considerably weaker, to a degree at which observation by PIV is not possible.

Fig. 9 shows the evolution of the maximum velocity fluctuations ( $u'_{rms}$  and  $v'_{rms}$ ) along the chord and reveals rapid increase of the maximum fluctuations as previously observed. A number of effects can be observed here: firstly, the amplification of both controlled and uncontrolled cases is high over most part of the FOV as evident by fluctuation intensity which is consistently larger than 1 % of the freestream velocity. This can lead to non-linear interaction of the developing TS modes and has implications on the working of the closed-loop control system as will be shown in the next section.

The dependence of the amplification on the forcing frequency is noteworthy here. The unsteady forcing effect of the actuator results in the introduction of a single-frequency disturbance in the

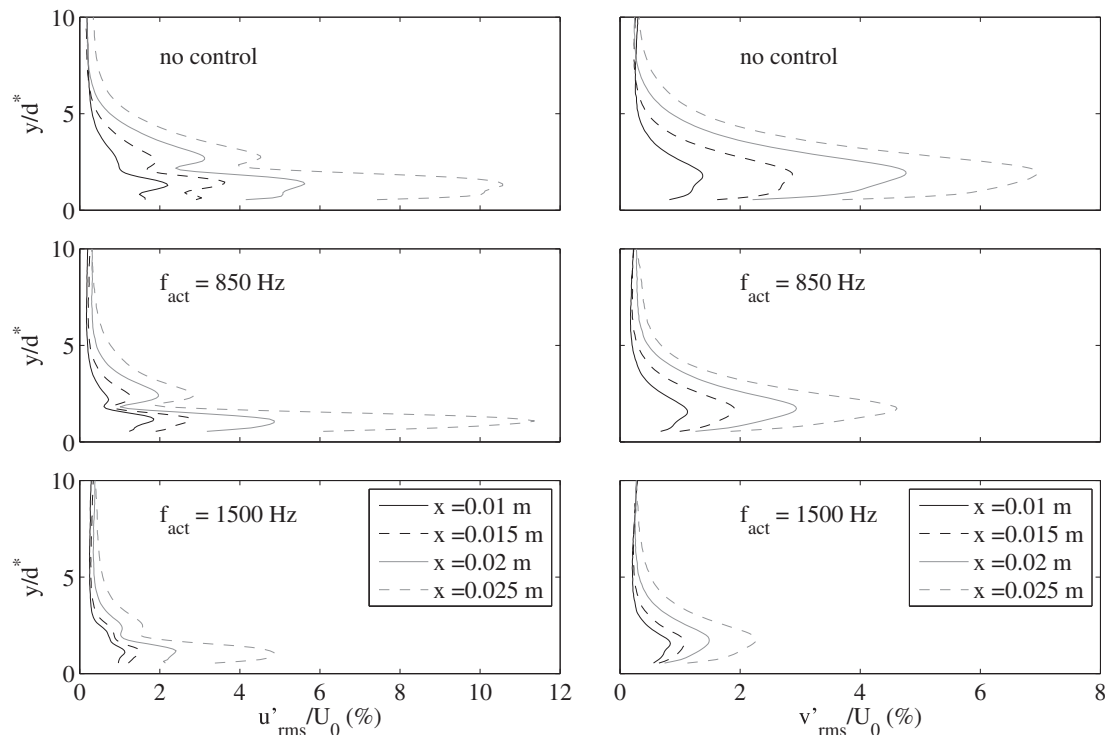


Figure 7. Velocity fluctuation ( $u'_{rms}$ ,  $v'_{rms}$ ) profiles for open-loop control ( $U_0 = 17$  m/s).

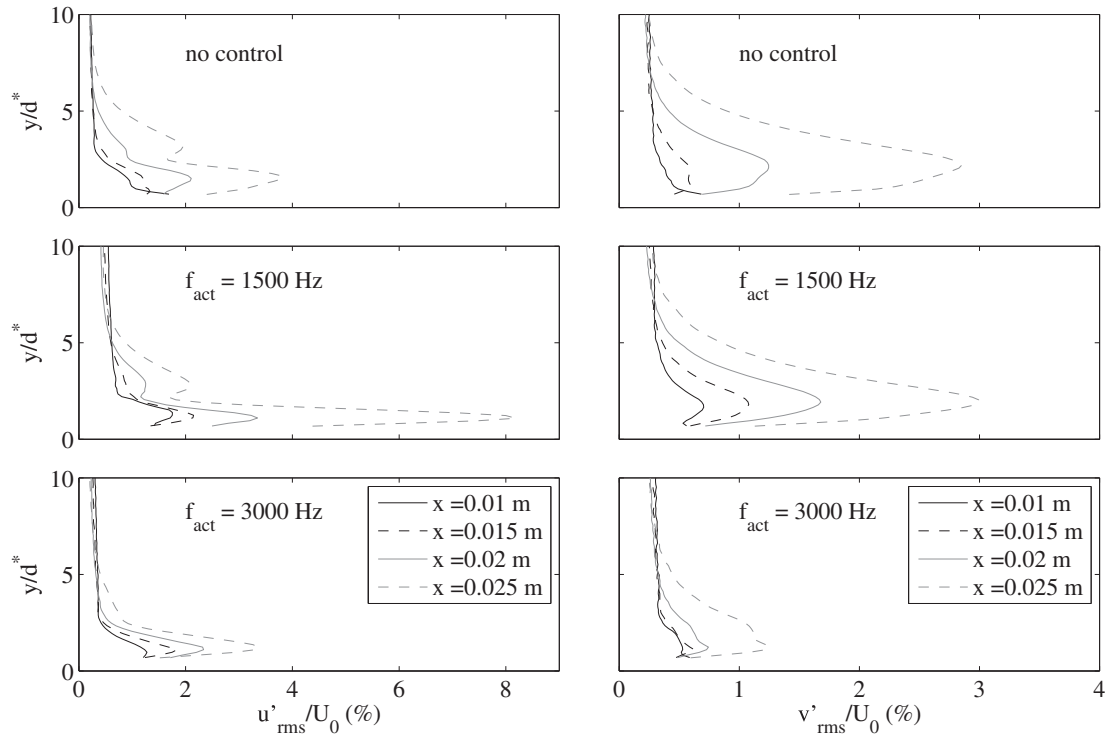


Figure 8. Velocity fluctuation ( $u'_{rms}$ ,  $v'_{rms}$ ) profiles for open-loop control ( $U_0 = 25$  m/s).

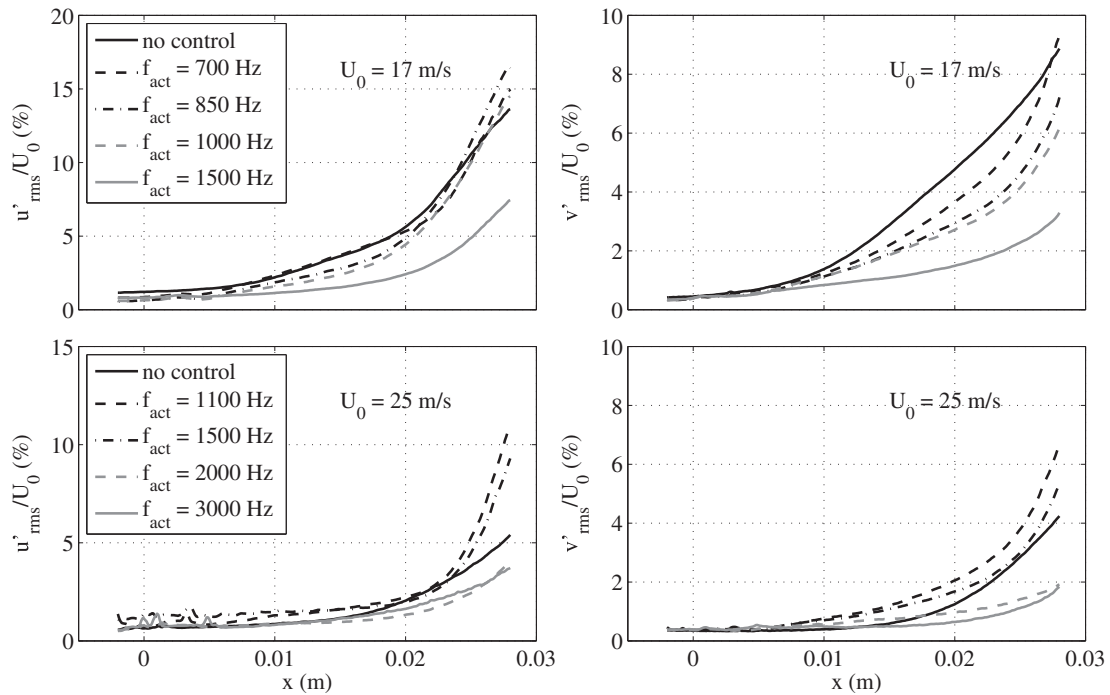


Figure 9. Streamwise evolution of the maximum value of velocity fluctuations for open loop control at  $U_0 = 17$  and  $25$  m/s respectively.

boundary layer. This is easier visualised by a spectral analysis of the velocity fluctuations. Fig. 10 shows power-spectral density (PSD) obtained through a modified periodogram analysis (Welch, 1967) of the velocity fluctuations sampled at the position of the error sensor ( $x = 10$  mm). Additionally, for the baseflow case, a Linear Stability Theory (LST) analysis has been performed using an Orr-Sommerfeld solver (van Ingen and Kotsonis, 2011). For this analysis, the experimentally measured

velocity profiles have been used at the location of the error sensor. Fig. 10 shows the local, imaginary part of the non-dimensional wavenumber. It must be noted here that direct comparison of the values of  $\alpha_i$  with the PSD should be avoided. The wave amplification can be retrieved from spatial integration of the imaginary wavenumber starting at the location of amplification onset. In the current study this is not readily available due to the limited FOV and as such the comparison serves only as an indication on the band of unstable frequencies expected at the conditions of the experiment.

A second mechanism, which is active here, is related to the time-averaged directional forcing effect due to the plasma actuator. This is typically manifested in quiescent flow conditions as a wall parallel jet (Moreau, 2007). In laminar boundary layer type flows this effect is manifested as the addition of momentum. The boundary layer becomes less inflectional and hence more stable. This is evident by the reduction of energy in the band of unstable frequencies for all actuation frequencies in Fig. 10. As such, the two concurrent mechanisms of steady and unsteady forcing can compete against each other in the case where the actuation frequency is within the unstable band.

This effect is especially pronounced in the case of  $U_0 = 25$  m/s (Fig. 11). Frequencies below 1500 Hz result in more amplified disturbances compared to the baseflow, since they lie in the unstable region. In contrast, forcing at higher frequencies such as 2000 and 3000 Hz, which for these conditions are in the stable region, in combination with the stabilising effect of the mean flow forcing, results in significant damping as evidenced by the RMS values in Fig. 9. It must be noted, that several peaks in Fig. 11 are artefacts of aliasing due to the close proximity of the forcing frequencies to the PIV sampling rate (indicated by grey color).

Finally, an effect can be observed related to the relative amplification in the streamwise and wall normal directions. As an example the case of  $f_{act} = 700$  Hz at  $U_0 = 17$  m/s (Fig. 9) can be examined. While the  $u'$  fluctuations increase compared to the no control case, the  $v'$  fluctuations reduce considerably. As such a *stretching* effect can be proposed that is attributed to the inherent forcing characteristics of the plasma actuator. This effect is evident in the closed-loop control case as well and further discussion is given in the following section.

Figure 12 shows a comparison of the time trace of velocity fluctuations ( $v'$ ) at the error microphone position for the cases of no actuation and control at 850 Hz and 1500 Hz. In the uncontrolled case, fluctuations occur in the form of wave packets. This is a typical characteristic of the development of natural TS waves where multiple frequency modes coexist in the developing boundary layer. When forcing is applied the developed unstable TS waves are locked to a single frequency corresponding to the actuation frequency. This is also evident in the PSD observations (Fig. 10). The reduction in intensity of velocity fluctuations shows the effective attenuation of TS waves at a carrier frequency of 1500 Hz due to the aforementioned steady forcing effect.

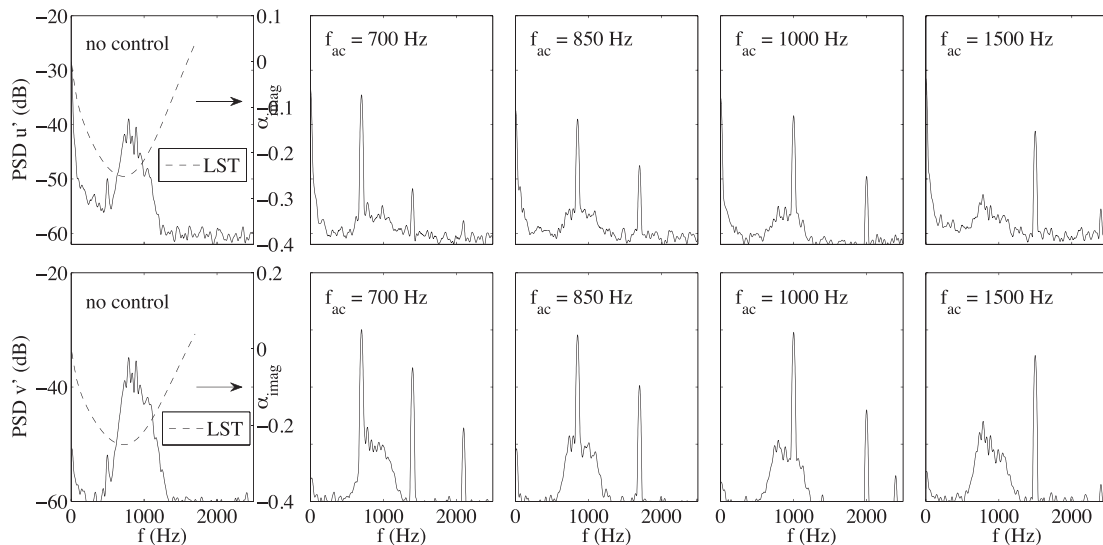


Figure 10. Power spectral density (PSD, arbitrary dB scale) of stream wise ( $u'$ ) and wall-normal ( $v'$ ) velocity fluctuations at  $x = 10$  mm,  $y = 2$  mm for open loop control ( $U_0 = 17$  m/s). The imaginary wavenumber for the no control case is calculated using LST based on the measured velocity profile.

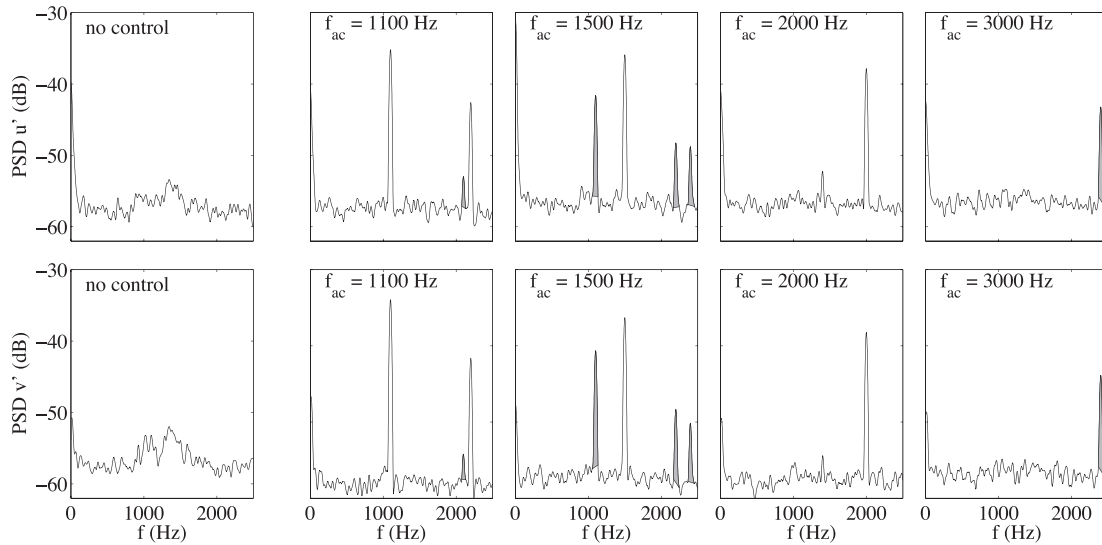


Figure 11. Power spectral density (PSD, arbitrary dB scale) of stream wise ( $u'$ ) and wall-normal ( $v'$ ) velocity fluctuations at  $x = 10$  mm,  $y = 2$  mm for open loop control ( $U_0 = 25$  m/s). The peaks marked with grey are artefacts due to aliasing and do not correspond to physical quantities.

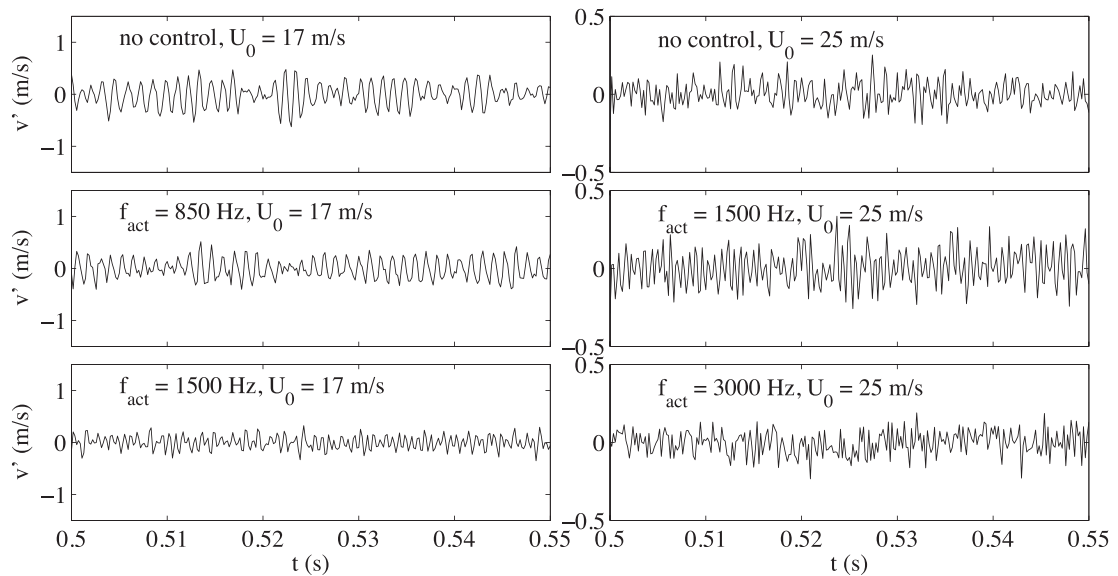


Figure 12. Time evolution of velocity fluctuations  $v'$  for open-loop control at  $U_0 = 17$  m/s (sampled at the error microphone).

#### 4.2. Closed-Loop Control

The Adaptive FXLMS control (closed-loop control) study is performed with the objective of controlling natural TS waves using a DBD plasma actuator. As mentioned earlier, a typical approach in plasma actuation is the modulation of a high frequency *carrier* signal with a lower *modulation* frequency in order to drive the HV power. The carrier signal is responsible for the production of the plasma, while the modulation is aimed at changing the magnitude of the plasma body force in order to oppose the incoming instabilities. A disadvantage of this technique is the requirement for the carrier and modulation frequencies to be sufficiently separated (by at least one order of magnitude) in order to preserve the forcing efficiency of the actuator and prevent introduction of spurious disturbances due to the carrier frequency fluctuation.

On the other hand, recent investigations have shown an inherently fluctuating behaviour for the plasma body force within the AC cycle of the HV signal (Kotsonis, and Ghaemi 2011). This periodic

fluctuation of the body force occurs at the carrier frequency and is attributed to the asymmetry in charged species population between the positive and negative half-cycle. This asymmetry can be exploited in active flow control of convective instabilities by completely eliminating the low frequency modulation and directly adapting the carrier signal. This approach has been used in the current work. The FXLMS controller autonomously selects the amplitude, phase and frequency of the HV signal.

#### 4.2.1. Controller characteristics

Three cases have been investigated at free stream velocities of 17, 20 and 25 m/s. The control sequence involved an initial system identification (SI) procedure followed by the adaptive control procedure. The primary FIR filter employs 50 taps (coefficients) while the convergence factor  $\beta$  is 0.3. These parameters were selected based on a parametric study on the controller's performance. The normalised coefficients of the primary FIR at the end of the PIV run are shown in Fig. 13. It is apparent that the FIR filter assumes the waveform of the incoming TS wave train. Additionally a reduction in the selected wavelength is consistent with the increase in free stream velocity.

Further insight in the operation of the controller is facilitated by the use of spectral analysis on the actuation signal. This is shown in Fig. 14 along with the spectra of the reference sensor. It should be noted that the signals have been normalised by the RMS value prior to the FFT analysis. As such, the actual amplitude in the PSD plot is not related to any physical quantity. It is evident that the controller is able to identify the broad range of unstable TS waves and match the spectral content of the actuation signal to this range.

The FIR coefficients (Fig. 13) and the PSD of the actuation signal (Fig. 14) suggest that the FXLMS controller is able to match the general form and spectral content of the incoming TS waves. Nevertheless, the principle of destructive interference via wave superposition necessitates the correct matching of the incoming phase as well. To verify this, a cross-correlation is performed on the signal of the reference microphone and the actuation signal. Similar to the spectral analysis, the cross-correlation coefficient is normalised by the product of standard deviation of the two signals. As such the degree of correlation is higher for values of the coefficient approaching 1. The cross-correlation coefficients are shown in Fig. 15 for the tested cases. It is apparent that significant matching of phase is achieved for a lag of several milliseconds. For larger lag the correlation degrades. This is indicative of the predictive capabilities and adaptation of the controller. The controller correctly matches the phase and frequency of the incoming wave for the time the latter needs to travel from the reference sensor to the actuator. This is manifested as strong correlation for three to six wavelengths, depending on freestream velocity (Fig. 15).

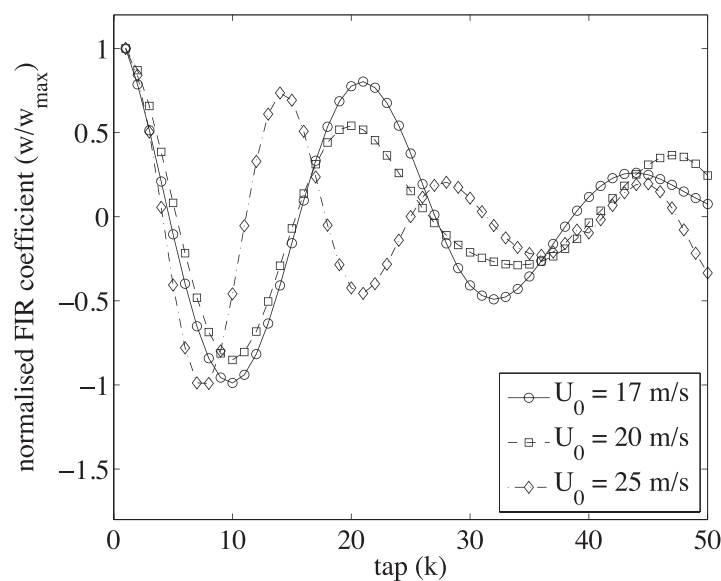


Figure 13. Coefficients of the primary FIR filter ( $w$ ) for the three tested free stream velocities. The coefficients have been normalised with their maximum.

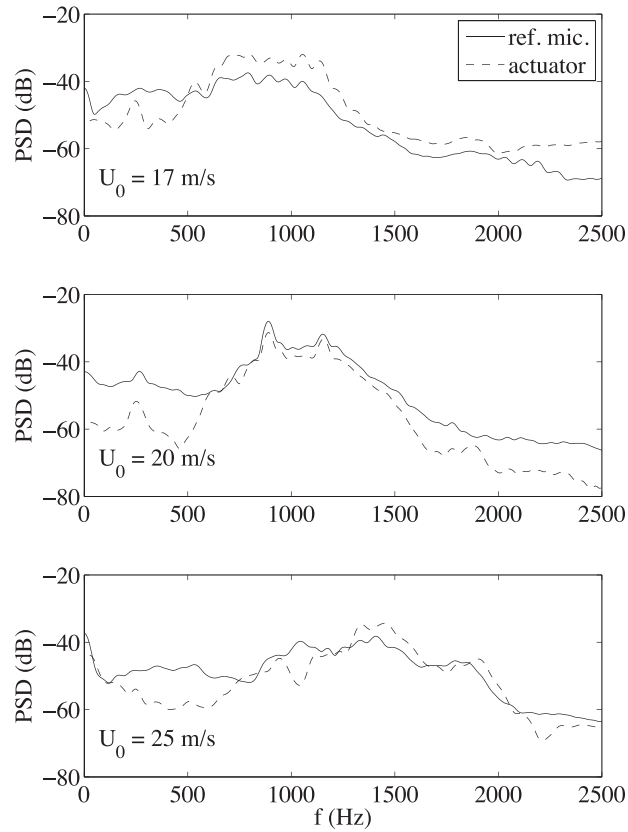


Figure 14. PSD of the actuation signal and reference microphone for the tested closed-loop cases (The signals have been normalised by their RMS value prior to the FFT procedure).

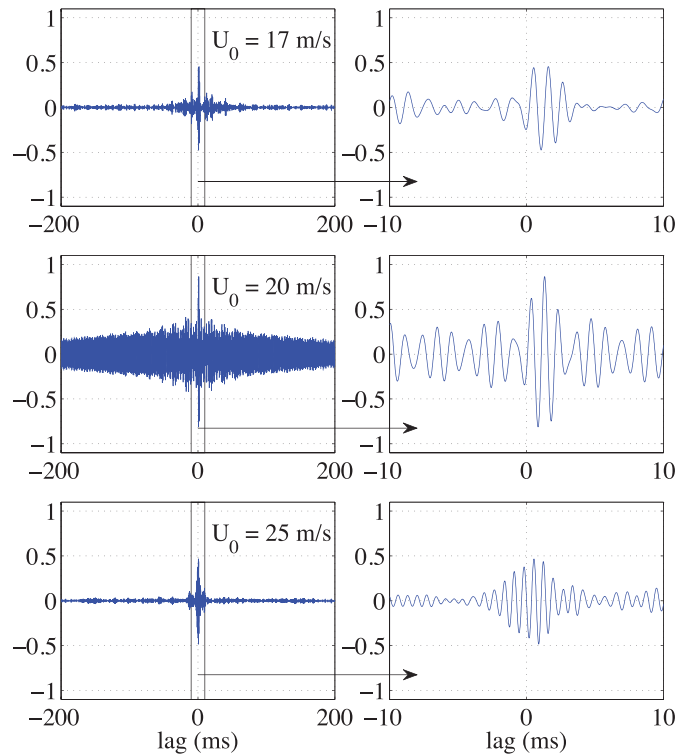


Figure 15. Cross-correlation of reference microphone signal and actuation signal for closed-loop control at the tested freestream velocities. Grey rectangle denotes the area shown in the right hand side.

Furthermore, the very short correlation length (a few wavelengths) suggests that a continuous adaptation of frequency and phase of the actuation signal is necessary in order to successfully sustain destructive interference throughout the operation time span.

4.2.2. Flowfield characteristics

Contours of wall-normal velocity fluctuations for uncontrolled and controlled cases are shown in Fig. 16. A reduction of fluctuation intensity is observed in all cases. Selected profiles of both streamwise and wall-normal velocity fluctuations are shown in Fig. 17. Additionally, the evolution of the maximum RMS fluctuations along the streamwise direction are shown in Fig. 18.

A similar effect to the open loop control can be highlighted here. The apparent reduction in fluctuating velocities appears to be higher for the wall normal component ( $v'$ ) compared to the

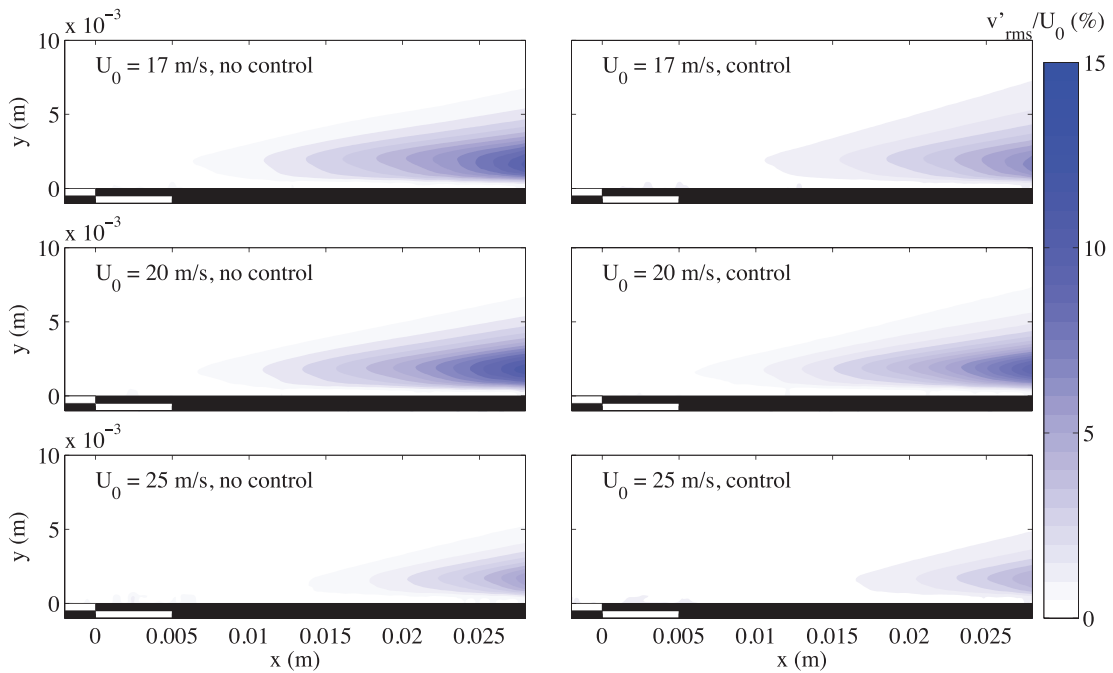


Figure 16. RMS of wall normal velocity fluctuations ( $v'_{rms}$ ) contours for closed-loop control at the three tested free stream velocities.

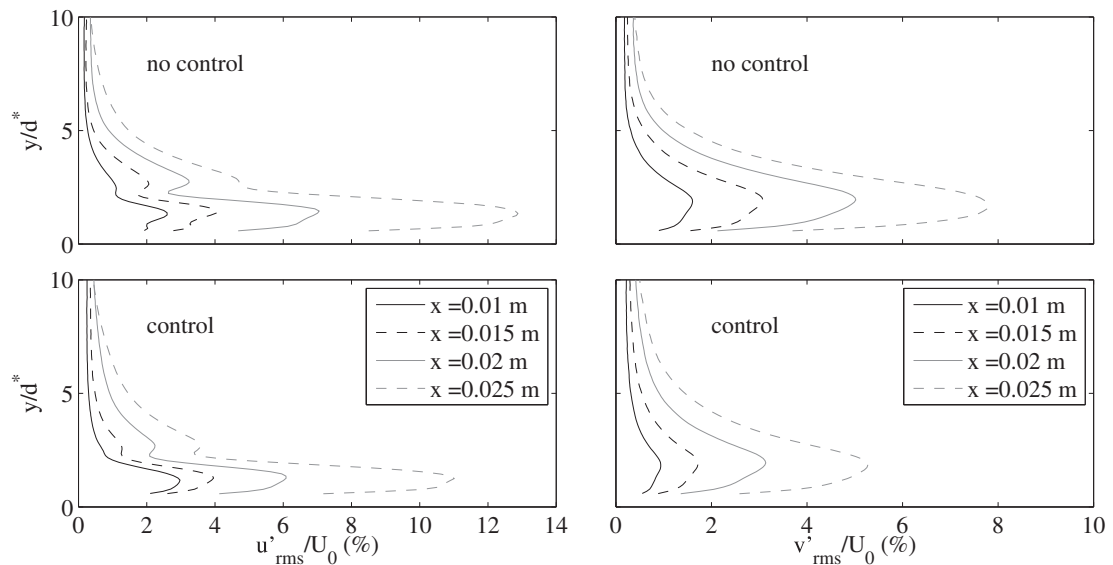


Figure 17. Velocity fluctuation ( $u'_{rms}$ ,  $v'_{rms}$ ) profiles for closed-loop control ( $U_0 = 17$  m/s).

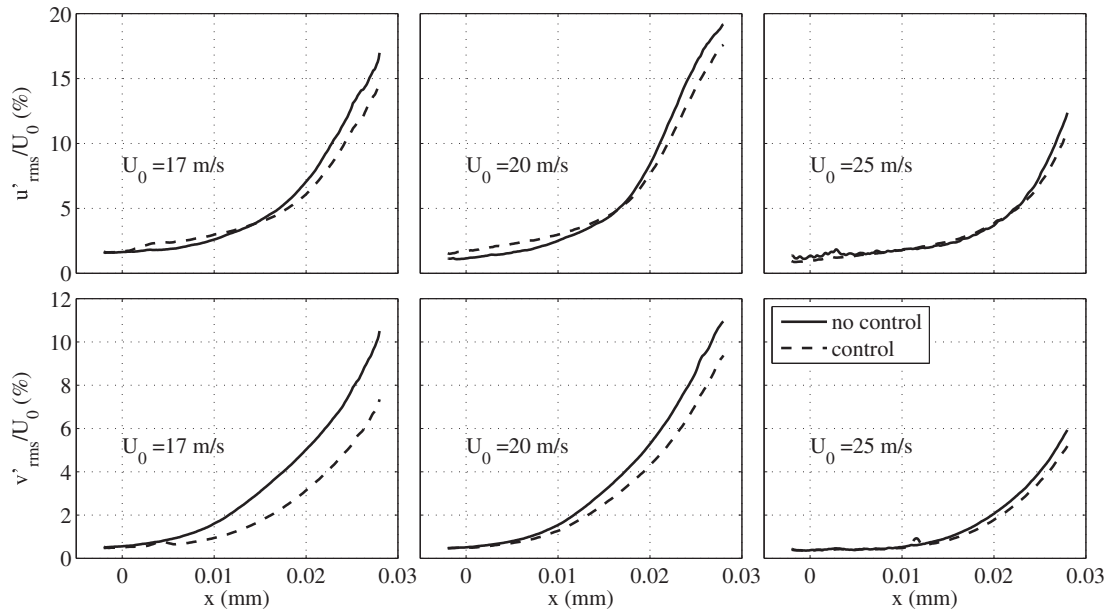


Figure 18. Comparison of the streamwise evolution of maximum velocity fluctuations in streamwise ( $u'_{rms}$ ) and wall-normal ( $v'_{rms}$ ) directions for all closed-loop cases.

streamwise component ( $u'$ ). It is apparent that although the overall TS wave fluctuation is suppressed, a stretching effect in the streamwise direction is present. This can be traced back to the effect of the actuator, since measurements of the body force distribution using PIV (Kotsonis et al., 2011b) have shown the force to be strongly aligned in the streamwise direction. Additionally, the previously mentioned periodic fluctuation of the force exerted on the fluid is not entirely symmetrical. The body force during the negative half-cycle is generally larger than the body force during the positive one, creating a net effect directed downstream. The total force can then be perceived as a steady DC component with an unsteady AC component.

From this point of view, stretching of the TS waves under plasma actuation can be attributed to the DC component of the dominantly streamwise body force. The wall normal fluctuations appear unaffected due to the significantly weaker wall-normal force. On the other hand, in the later stages of transition the instability modes evolve in the form of vortical structures. As such, the streamwise and wall-normal fluctuations are inherently coupled. The AC action of the actuator on the streamwise fluctuation component is transferred via this coupling to the wall-normal component with the corresponding attenuation effect.

The spectra of wall-normal velocity fluctuations are presented in Fig. 19. TS waves grow within a narrow band as dictated by the stability characteristics of the present boundary layer. Within this band, the controller is able to reduce the intensity of the fluctuations by  $-10$  dB at  $U_0 = 17$  m/s. It should be noted that the strong peaks at the forcing frequency and their harmonics are not present here in contrast to the open loop case. This is attributed to the continuous adaptation of the control signal, such that the plasma force directly opposes the incoming instabilities, as previously described. Due to the matching of phase and frequency of the actuation signal to that of the flow instabilities, the control action introduces very little harmonic spectral content in the flow. For the higher velocities, attenuation is also observed albeit not as striking as for 17 m/s. Time traces of the fluctuating wall normal velocities are shown in Fig. 20.

## 5. CONCLUSION

An experimental study of the active control of naturally occurring Tollmien-Schlichting (TS) instabilities on a NACA 0012 airfoil was carried out. A closed-loop control system using the filtered-x Least Mean Squares adaptive algorithm based on Finite Impulse Response filters is successfully applied to achieve attenuation of naturally occurring TS instabilities. Results indicate the attenuation of energy in the band associated to unstable TS waves with closed-loop actuation. Reduction in amplitude of approximately 50% is achieved for the free stream velocity of 17 m/s, while some suppression is maintained for higher velocities.

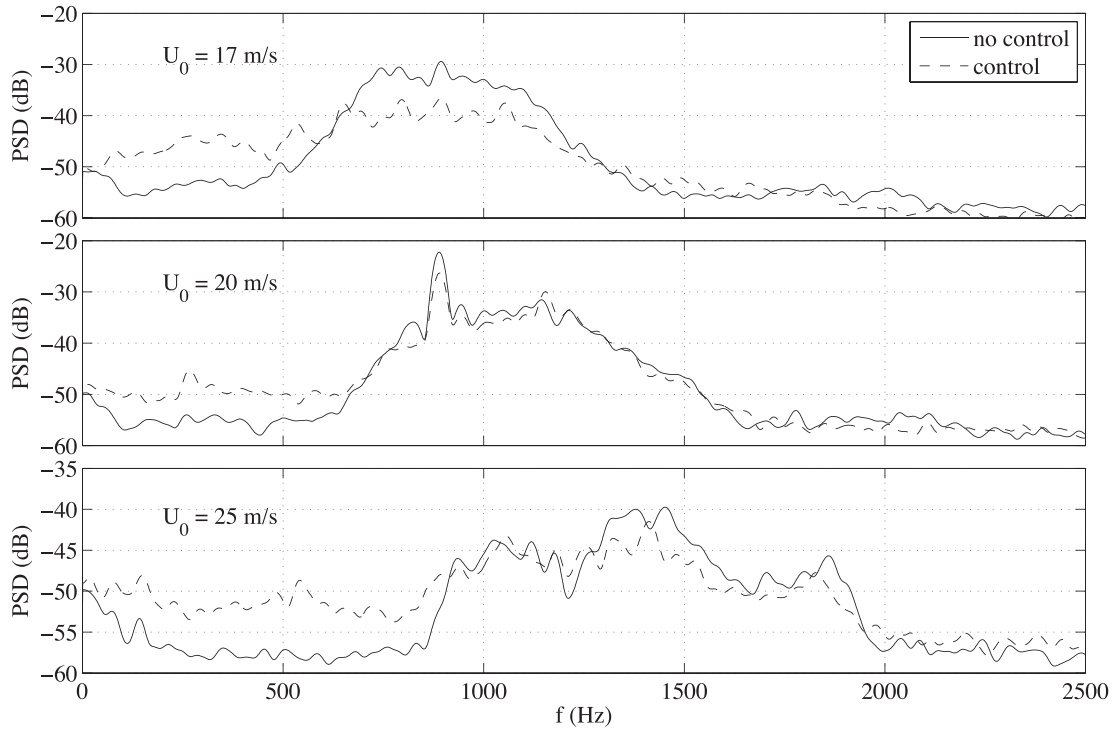


Figure 19. PSD of wall-normal velocity fluctuations sampled above the error signal for closed-loop control case at  $U_0 = 17, 20$  and  $25$  m/s.

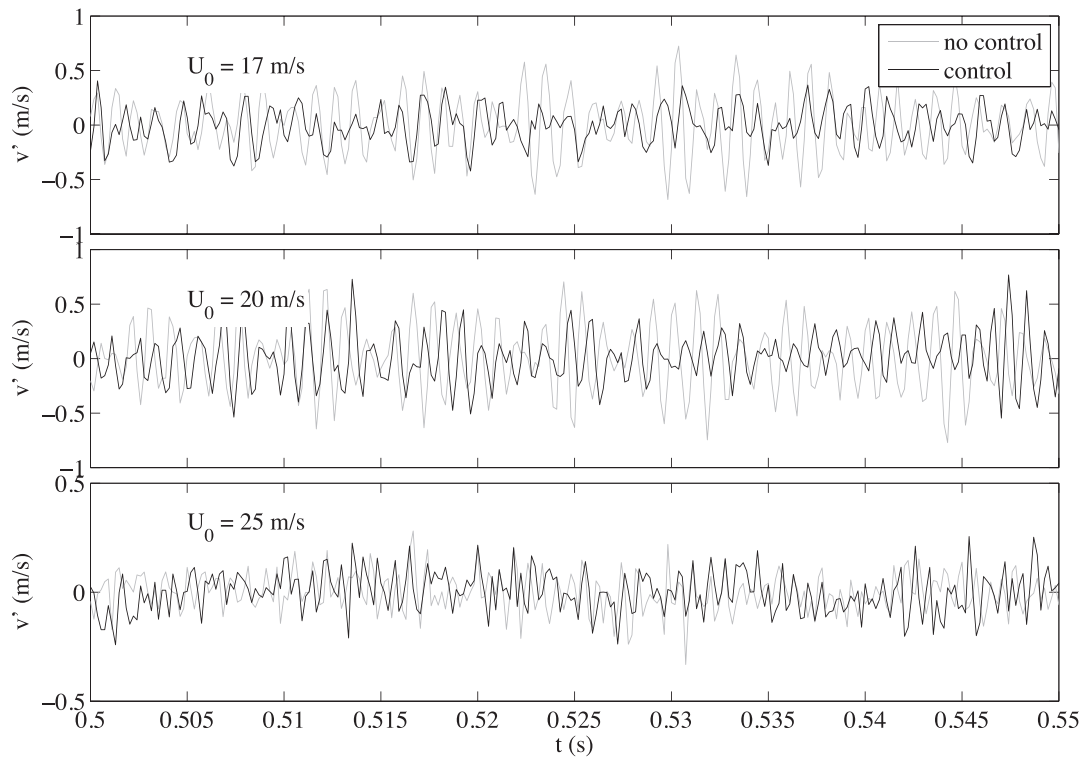


Figure 20. Time evolution of velocity fluctuations ( $v'$ ) for closed-loop control at the three tested freestream velocities. Time trace is sampled 1 mm above the error microphone position ( $x = 10$  mm).

It is interesting to note the fundamental differences between the open- and closed-loop control approaches. With open-loop control the actuation is performed at a fixed frequency, phase and amplitude. As such the actuator is introducing discrete perturbations in the flow, which can either grow or decay depending on the natural stability of the boundary layer. Additionally, harmonics of the actuation frequency are observed in the velocity trace, which can potentially grow downstream. On the other hand, in cases where the actuation frequency is in the vicinity or outside of the neutral stability curve, flow instability is suppressed. This can be attributed to the quasi-steady forcing of the actuator, which results in the addition of momentum to the boundary layer, thus rendering the latter more stable.

The closed-loop control case presents particularities, which are inherent to the workings of adaptive control algorithms like FXLMS. The energy content in the frequency band associated to the unstable TS waves downstream of the actuator is significantly lower than for open-loop control. This demonstrates the ability of the controller to match frequency and phase of the incoming instability and to adjust the amplitude such that overall attenuation is achieved. This is further verified by strong correlation of the reference signal and the actuation signal for short phase lags.

Direct use of the carrier voltage signal to drive the actuator is demonstrated as an alternative to the more commonly used modulated sinusoidal waveform. The inherently unsteady behaviour of the produced body force can be directly used as a control mechanism. This approach has significant merit for higher Reynolds numbers. Indeed, considering the current study, at  $U_0 = 25$  m/s the range of unstable TS wave frequencies is in the order of kilohertz. For industrially relevant applications this range can be well in the tens of kilohertz. At such frequencies, the modulation approach becomes severely impractical. On the other hand, direct adaptation of the carrier signal can provide the means for efficient actuation. Moreover, recent work of Kotsonis and Ghaemi (2012) has shown the significant influence the waveform shape has on the unsteady forcing behaviour of the actuator. This can be further exploited via dynamic adaptation of the magnitude of applied voltage in addition to phase, frequency and amplitude.

## REFERENCES

- [1] Albrecht, T., Grundmann, R., Mutschke, G. and Gerbeth, G., 2006. On the stability of the boundary layer subject to a wall-parallel Lorentz force. *Phys. Fluids* 18(9), 098103.
- [2] Baumann, M. and Nitsche, W., 1996. Investigation of active control of Tollmien-Schlichting waves on a wing. In: Henkes, R., van Ingen, J. (Eds.), *Transitional Boundary Layers in Aeronautics*, Vol. 46. KNAW, Amsterdam, Netherlands, pp. 89–98.
- [3] Baumann, M. and Nitsche, W., 1997. Experiments on active control of Tollmien-Schlichting waves on a wing. In: Korner, H., Hilbig, R. (Eds.), *New Results in Numerical and Experimental Fluid Mechanics*, Vol. 60 of NNFM. Vieweg Verlag, Braunschweig, pp. 56–63.
- [4] Baumann, M., Sturzebecher, D. and Nitsche, W., 2000. Active control of TS-instabilities on an unswept wing. In: Fasel, H., Saric, W. (Eds.), *Laminar-Turbulent Transition*, IUTAM Symposium Sedona/AZ 1999. Springer-Verlag, pp. 155–160.
- [5] Gmelin, C., Rist, U. and Wagner, S., 2000. DNS of active control of disturbances in a blasius boundary layer. In: Fasel, H., Saric, W. (Eds.), *Laminar-Turbulent Transition*, IUTAM Symposium Sedona/AZ 1999. Springer-Verlag, pp. 149–154.
- [6] Grundmann, S. and Tropea, C., 2008. Active cancellation of artificially introduced tollmien-schlichting waves using plasma actuators., *Experiments in Fluids* 44(5), 795–806.
- [7] Herbert, T., Fan, X. and Haritonidis, J., 1996. Laminar flow control with neural networks. *ASME Papers FED-Vol. 242*, Proceedings of the ASME Fluids Engineering Division, pp. 87–91.
- [8] Hansen, C., 2001. *Understanding Active Noise Cancellation*, Taylor and Francis.
- [9] Joslin, R., Nicolaidis, R., Erlebacher, G., Hussaini, M. and Gunzburger, M., 1995, Active control of boundary layer instabilities: use of sensors and spectral controller., *AIAA J.* 33(8).
- [10] Kotsonis, M and Ghaemi, S., 2011. Forcing mechanisms of dielectric barrier discharge plasma actuators at carrier frequency of 625 Hz. *Journal of Applied Physics* 110 (11), 113301.
- [11] Kotsonis, M., Ghaemi, S., Veldhuis, L., and Scarano, F., 2011b. Measurement of the body force field of plasma actuators. *Journal of Physics D: Applied Physics*, 44(4).
- [12] Kotsonis, M., and Ghaemi, S. 2012. Performance improvement of plasma actuators using asymmetric high voltage waveforms. *Journal of Physics D: Applied Physics*, 45(4).

- [13] Kotsonis, M., Giepmans, R., Hulshoff, S. and Veldhuis, L. 2013. Numerical study of the control of Tollmien-Schlichting waves using plasma actuators. *AIAA Journal*, 51(10), 2353–2364.
- [14] Kuo, S. and Moran, D., 1996, Active noise control systems, John Wiley, New York.
- [15] Kurz, A., Tropea, C., Grundmann, S., Forte, M., Vermeersch, O., Seraudie, A. and King, R., 2012. Transition delay using DBD plasma actuators in direct frequency mode. Paper presented at the *6th AIAA Flow Control Conference 2012*.
- [16] Liepmann, H. and Nosenchuck, D., 1982, Active control of laminar-turbulent transition., *Journal of Fluid Mechanics* 118(1), 201–204.
- [17] Ladd, D. and Hendricks, E., 1988. Active control of 2-D instability waves on an axisymmetric body. *Exp. Fluids* 6, 69–70.
- [18] Ladd, D., 1990. Control of natural instability waves on an axisymmetric body. *AIAA J.* 28(2), 367–369.
- [19] Milling, R., 1981, ‘Tollmien-Schlichting wave cancellation.’, *Physics of Fluids* 24, 979.
- [20] Moreau, E. 2007. Airflow control by non-thermal plasma actuators. *Journal of Physics D: Applied Physics*, 40(3), 605–636.
- [21] Plogmann, B., Herrig, A. and Würz, W. 2013. Experimental investigations of a trailing edge noise feedback mechanism on a NACA 0012 airfoil. *Experiments in Fluids*, 54(5).
- [22] Pröbsting, S., Serpieri, J. and Scarano, F. 2014. Experimental investigation of aerofoil tonal noise generation. *Journal of Fluid Mechanics*, 747(2), 656–687.
- [23] Pupator, P. and Saric, W., 1989. Control of random disturbances in a laminar boundary layer. *AIAA Paper* 89–1007.
- [24] Sturzebecher, D. and Nitsche, W. 2003. Active cancellation of Tollmien-Schlichting instabilities on a wing using multi-channel sensor actuator systems., *International Journal of Heat and Fluid Flow* 24(4), 572–583.
- [25] Thomas, A. 1983, The control of boundary-layer transition using a wave-superposition principle., *Journal of Fluid Mechanics* 137, 233–250.
- [26] Van Ingen, J. and Kotsonis, M., 2011. A two-parameter method for eN transition prediction. Paper presented at the *6th AIAA Theoretical Fluid Mechanics Conference*.
- [27] Welch, P.D., 1967. The Use of Fast Fourier Transform for the Estimation of Power Spectra: A Method Based on Time Averaging Over Short, Modified Periodograms., *IEEE Transactions on Audio Electroacoustics*, AU-15, 70–73.